NASA TECHNICAL NOTE

NASA TN D-3915

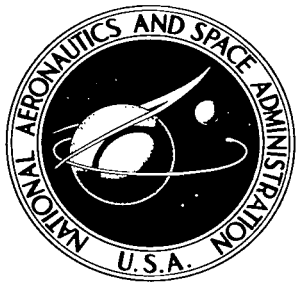

LONGITUDINAL AERODYNAMIC CHARACTERISTICS OF SEVERAL HIGH-DRAG BODIES AT MACH NUMBERS FROM 1.50 TO 4.63

by James F. Campbell

Langley Research Center

Langley Station, Hampton, Va.

NATIONAL AERONAUTICS AND SPACE ADMINISTRATION • WASHINGTON, D. C. • APRIL 1967

LONGITUDINAL AERODYNAMIC CHARACTERISTICS OF SEVERAL HIGH-DRAG BODIES AT MACH NUMBERS FROM 1.50 TO 4.63

By James F. Campbell

Langley Research Center
Langley Station, Hampton, Va.

NATIONAL AERONAUTICS AND SPACE ADMINISTRATION

For sale by the Clearinghouse for Federal Scientific and Technical Information
Springfield, Virginia 22151 – CFSTI price $3.00

LONGITUDINAL AERODYNAMIC CHARACTERISTICS OF SEVERAL HIGH-DRAG BODIES AT MACH NUMBERS FROM 1.50 TO 4.63

By James F. Campbell
Langley Research Center

SUMMARY

An investigation has been conducted at Mach numbers from 1.50 to 4.63 to determine the static longitudinal aerodynamic characteristics of several high-drag entry bodies. A 100° cone, a 120° cone, and a tension-shell-shape model were tested at angles of attack to about 50°; most of these tests were performed at a Reynolds number based on model diameter of 2.0×10^6.

The results of the investigation indicated that all three configurations are statically stable at low angles of attack in the test Mach number range and that the two cones are stable throughout the entire test angle-of-attack range. The tension-shell model, however, produces highly nonlinear variations of pitching moment, lift, and drag at angles of attack beyond about ±2° for Mach numbers above 1.90. These nonlinearities are caused by asymmetrical shock patterns and would probably lead to unsatisfactory stability characteristics for a vehicle following a zero-lift trajectory. The axial-force (and drag) coefficient for the 120° cone is generally greater than for the other two test vehicles throughout the Mach number range.

INTRODUCTION

The National Aeronautics and Space Administration is presently involved in study programs to determine suitable shapes for vehicles entering planetary atmospheres and also shapes for aerodynamic braking to decelerate from hypersonic to subsonic speeds. In many ways these programs intermesh since the need for high drag values and low structural mass are major requirements of both programs. Considerable information on vehicles of this type is available and some may be found in references 1 to 6. More recently high-angle cones and tension-shell shapes have become of interest because of their inherently high drag and good structural weight characteristics; however, results are meager in the supersonic speed regime on these types of vehicles. In addition, some results (ref. 7) have indicated that cones with nose angles greater than 90° have undesirable stability characteristics as towed decelerators. These higher angle cones, however, may possibly be suitable vehicles for entry into planetary atmospheres. It was therefore

believed desirable to determine the static longitudinal aerodynamic characteristics of a 100° and 120° cone and also of a "tensoid-shape" model in the supersonic speed range. The tensoid shape is defined as a tension shell of revolution having negative Gaussian curvature and supported at the base by a compression ring. The results of tests on these three configurations are presented herein for Mach numbers from 1.50 to 4.63 and at angles of attack to about 50°. Most of these tests were performed at a Reynolds number based on model diameter of 2.0×10^6.

SYMBOLS

The data are referred to both the body- and stability-axis systems with moments for each model taken about the center-of-gravity locations shown in figure 1.

Measurements for this investigation were taken in the U.S. Customary System of Units. Equivalent values are indicated herein parenthetically in the International System (SI) in the interest of promoting use of this system in future NASA reports. Details concerning the use of SI, together with physical constants and conversion factors, are given in reference 8.

A base area of model

C_A axial-force coefficient, $\frac{\text{Axial force}}{qA}$

C_D drag coefficient, $\frac{\text{Drag}}{qA}$

C_L lift coefficient, $\frac{\text{Lift}}{qA}$

C_m pitching-moment coefficient, $\frac{\text{Pitching moment}}{qAD}$

C_N normal-force coefficient, $\frac{\text{Normal force}}{qA}$

$C_{L_\alpha} = \frac{\partial C_L}{\partial \alpha}$, per degree

$C_{m_\alpha} = \frac{\partial C_m}{\partial \alpha}$, per degree

$C_{N_\alpha} = \frac{\partial C_N}{\partial \alpha}$, per degree

D base diameter of model

M free-stream Mach number

Δp	difference between local static pressure and free-stream static pressure
q	free-stream dynamic pressure
r	radial coordinate of model
x	axial coordinate of model, forward of base (fig. 1)
α	angle of attack

Subscript:

0	conditions at zero angle of attack

APPARATUS AND METHODS

Models

Dimensional drawings of the test models are shown in figure 1. The models, consisting of a 100° cone, a 120° cone, and a tensoid shape, were constructed of polished aluminum. Coordinates for the tensoid model are given in table I.

Tunnel

Tests were conducted in the low and high Mach number test sections of the Langley Unitary Plan wind tunnel, which is a variable-pressure continuous-flow tunnel. The test sections are 4 feet (1.22 meters) square and 7 feet (2.13 meters) long. The nozzles leading to the test sections are of the asymmetric sliding-block type which permits a continuous variation in Mach number from 1.5 to 2.9 in the low Mach number test section and from about 2.3 to 4.7 in the high Mach number test section.

Test Conditions

The models were tested at Mach numbers from 1.50 to 4.63 through an angle-of-attack range of -6° to 50° at zero sideslip. All models were tested with a transition strip on the nose. The strip was composed of No. 60 carborundum particles affixed to the models as a 1/16-inch (0.159-cm) band located 1.2 inches (3.0 cm) along the model surface measured from the nose center line.

Reynolds number based on model diameter was 2.0×10^6 for these tests, except at $M = 1.50$ and 1.90, where the Reynolds number was 1.667×10^6 for the 100° and 120° cone configurations and 1.790×10^6 and 1.370×10^6, respectively, for the tensoid shape.

Stagnation dewpoint was maintained at -30° F (239° K) to avoid condensation effects in the test sections.

Measurements, Corrections, and Accuracy

Aerodynamic forces and moments were measured by means of an electrical strain-gage balance housed partially in the models. The aft end of the balance which extended behind the base of the models was enclosed in a sleeve, so that it was protected from any flow gradients. Schlieren photographs of many of the attitudes of the three models were obtained, and typical photographs are presented in figures 2, 3, and 4 for the 100° cone, 120° cone, and tensoid shape, respectively.

Angles of attack have been corrected for both tunnel-flow angularity and deflection of the balance and sting due to aerodynamic loads. No corrections have been made to the axial-force or drag results to account for balance chamber or model-base pressure. Chamber pressure coefficients for $\alpha \approx 0^{\circ}$, however, are given in table II.

Based upon calibration and repeatability of data, the various measured quantities are estimated to be accurate within the following limits:

C_A	±0.010
C_D	±0.010
C_L	±0.010
C_m	±0.002
C_N	±0.010
α, deg	±0.100
Mach 1.50 to 2.96	±0.015
Mach 3.95 to 4.63	±0.050

RESULTS AND DISCUSSION

The basic aerodynamic characteristics in pitch for the three test configurations are presented in figures 5 and 6 for the body and stability axes, respectively. Data are presented for both axes systems because the high axial-force levels of the vehicles greatly affect the variation of lifting characteristics with angle of attack. The normal-force and pitching-moment data for the cones are relatively linear with angle of attack throughout the test Mach number range (fig. 5), both configurations being statically stable. The slope of the normal-force curve for the 100° cone through $\alpha \approx 0^{\circ}$ is considerably greater than for the 120° cone and, in addition, the 100° cone develops more positive normal force up to the highest positive test angle of attack throughout the range of test Mach numbers. Virtually no effect of Mach number is noted on C_{N_α} for the 120° cone. (See summary plot of fig. 7.)

The 120^{o} cone develops a significantly higher axial force than does the 100^{o} cone at all test Mach numbers. As would be expected, C_A at $\alpha = 0^{o}$ increases with increase in Mach number for the 100^{o} cone (fig. 7) until the Mach number is reached at which shock attachment occurs (approximately 3.2); further increase in Mach number is accompanied by a decrease in $C_{A,0}$ for this configuration. Since the shock remains unattached for the 120^{o} cone at all Mach numbers, its value of $C_{A,0}$ increases with any increase in Mach number, though the effect is only slight at Mach numbers above about 2.3. The axial-force data at $M = 1.50$ are considered questionable because of the proximity of the tunnel normal shock wave to the model base.

The normal-force data for the tensoid-shape model at the two lower test Mach numbers are intermediate to those for the cones in the lower angle-of-attack range (fig. 5). In the higher angle-of-attack range at $M = 1.50$ and 1.90 there is an increase in C_{N_α} for this configuration which is reflected in a sharp stabilizing trend. The angle of attack for this stabilizing trend (or increased C_{N_α}) is considerably lower at $M = 1.90$ than at $M = 1.50$. With further increase in Mach number, the tensoid model develops a sharp increase in C_{N_α} in the angle-of-attack range of about $\pm 2^{o}$, this increase being accentuated with increase in Mach number (note summary plot, fig. 7) and reflected in a large increase in the stability level of the vehicle in this low α-region. The C_{N_α} at angles of attack above about 2^{o} reduces drastically at all Mach numbers above 1.90 leading to discrete ranges of angle of attack where C_{m_α} becomes either zero or positive. In the high angle-of-attack range, the stability level of the vehicle again increases rapidly. The nonlinearity of these data would probably lead to unsatisfactory stability characteristics for a tensoid-shape vehicle following a zero-lift trajectory. An examination of the schlieren photographs (fig. 4) indicates that at $M = 1.50$ there is a bow wave forward of the model at all test angles of attack. At $M = 1.90$ (fig. 4(b)), in the lower angle-of-attack range, there is a small portion of the nose where the bow wave follows the nose contour. Separation of the flow over the aft portions of the model causes a strong bow wave which merges with the forward bow wave. At high angles of attack, the discontinuity caused by this merger disappears. With further increase in Mach number, the shock wave on the nose moves farther back on the model before merging with the bow wave (at angles of attack near 0^{o}) and this phenomenon probably causes the large increase in C_{m_α}. With increase in angle of attack, however, the bow wave becomes unsymmetrical because of nonsymmetrical flow separation that leads to the aforementioned decrease in C_{m_α}. At high angles of attack, the bow wave becomes continuous (i.e., not a merger of two waves) and leads to stable conditions for the model. The large reductions in axial-force coefficient at the higher Mach numbers for α near 0^{o} are believed to be caused by the separation of flow on the model face. This separation essentially induces a new model profile which is almost conical and leads to a conical shock wave rather than the familiar bow wave. This, in turn, leads to a reduction in drag coefficient. With increase

in angle of attack, a rather conventional bow wave appears on the windward side of the model and at high angles of attack this wave is well forward of the complete model. The variation of axial-force coefficient ($\alpha = 0^{o}$) with Mach number is seen in figure 7.

The slopes of the curves of lift coefficient as a function of angle of attack for the 100^{o} and 120^{o} cone configurations are negative throughout the test Mach number range because of the large component due to axial force (fig. 6). This result is also noted in data such as that of reference 1 which indicates that negative lift-curve slopes are obtained for cones with included apex angles greater than 90^{o}. In addition, the 120^{o} cone, because of its greater axial force, has a greater negative C_{L_α} than does the 100^{o} cone model. At $M = 1.50$ and 1.90 (fig. 6), C_{L_α} for the tensoid shape is also negative and relatively linear to angles of attack of 30^{o} and 20^{o}, respectively. At higher Mach numbers, however, nonlinearities become pronounced and C_{L_α} in the angle-of-attack range of about $\pm 2^{o}$ becomes increasingly positive as a result of the reduced axial force in that region.

CONCLUDING REMARKS

Wind-tunnel tests of a 100^{o} cone, a 120^{o} cone, and a tensoid-shape model at Mach numbers from 1.50 to 4.63 lead to the following observations:

All three configurations are statically stable at low angles of attack in the test Mach number range and the two cones are stable throughout the entire test angle-of-attack range. The tensoid model, however, produces highly nonlinear variations of pitching moment, lift, and drag at angles of attack beyond about $\pm 2^{o}$ for Mach numbers above 1.90. These nonlinearities are caused by asymmetrical shock patterns and would probably lead to unsatisfactory stability characteristics for a vehicle following a zero-lift trajectory. The axial-force (and drag) coefficient is generally greater for the 120^{o} cone than for the other two test vehicles throughout the Mach number range.

Langley Research Center,
National Aeronautics and Space Administration,
Langley Station, Hampton, Va., November 8, 1966,
124-08-06-03-23.

REFERENCES

1. Penland, Jim A.: Aerodynamic Force Characteristics of a Series of Lifting Cone and Cone-Cylinder Configurations at a Mach Number of 6.83 and Angles of Attack up to 130^{o}. NASA TN D-840, 1961.

2. Owens, Robert V.: Aerodynamic Characteristics of Spherically Blunted Cones at Mach Numbers From 0.5 to 5.0. NASA TN D-3088, 1965.

3. Penland, Jim A.: A Study of the Stability and Location of the Center of Pressure on Sharp, Right Circular Cones at Hypersonic Speeds. NASA TN D-2283, 1964.

4. Bernot, Peter T.: Longitudinal Stability Characteristics of Several Proposed Planetary Entry Vehicles at Mach 6.73. NASA TN D-2785, 1965.

5. Robinson, James C.; and Jordan, Alfred W.: Exploratory Experimental Aerodynamic Investigation of Tension Shell Shapes at Mach 7. NASA TN D-2994, 1965.

6. Campbell, James F.: Flow Field Survey and Decelerator Drag Characteristics in the Wake of a Model of the X-15 Airplane at Mach 2.30 and 4.65. NASA TN D-3285, 1966.

7. Charczenko, Nickolai; and McShera, John T.: Aerodynamic Characteristics of Towed Cones Used as Decelerators at Mach Numbers From 1.57 to 4.65. NASA TN D-994, 1961.

8. Mechtly, E. A.: The International System of Units – Physical Constants and Conversion Factors. NASA SP-7012, 1964.

TABLE I.- COORDINATES DEFINING TENSOID-SHAPE MODEL

x/D	r/D
0	0.5000
.0015	.4750
.0070	.4500
.0150	.4250
.0265	.4000
.0415	.3750
.0590	.3500
.0800	.3250
.1045	.3000
.1310	.2750
.1610	.2500
.1927	.2250
.2295	.2000
.2670	.1750
.3075	.1500
.3495	.1250
.3935	.1000
.4385	.0750
.4850	.0500
.5325	.0250
.5800	0

TABLE II.- CHAMBER PRESSURE COEFFICIENTS

$[\alpha \approx 0^{o}]$

M	Chamber pressure coefficient $\frac{\Delta p}{q}$		
	100^{o} cone	120^{o} cone	Tensoid shape
1.50	-0.0164	-0.0471	-0.0034
1.90	-.1783	-.1893	-.1872
2.30	-.1447	-.1605	-.1971
2.96	-.1106	-.0973	-.1447
3.95	-.0705	-.0544	-.0870
4.63	-.0589	-.0348	-.0718

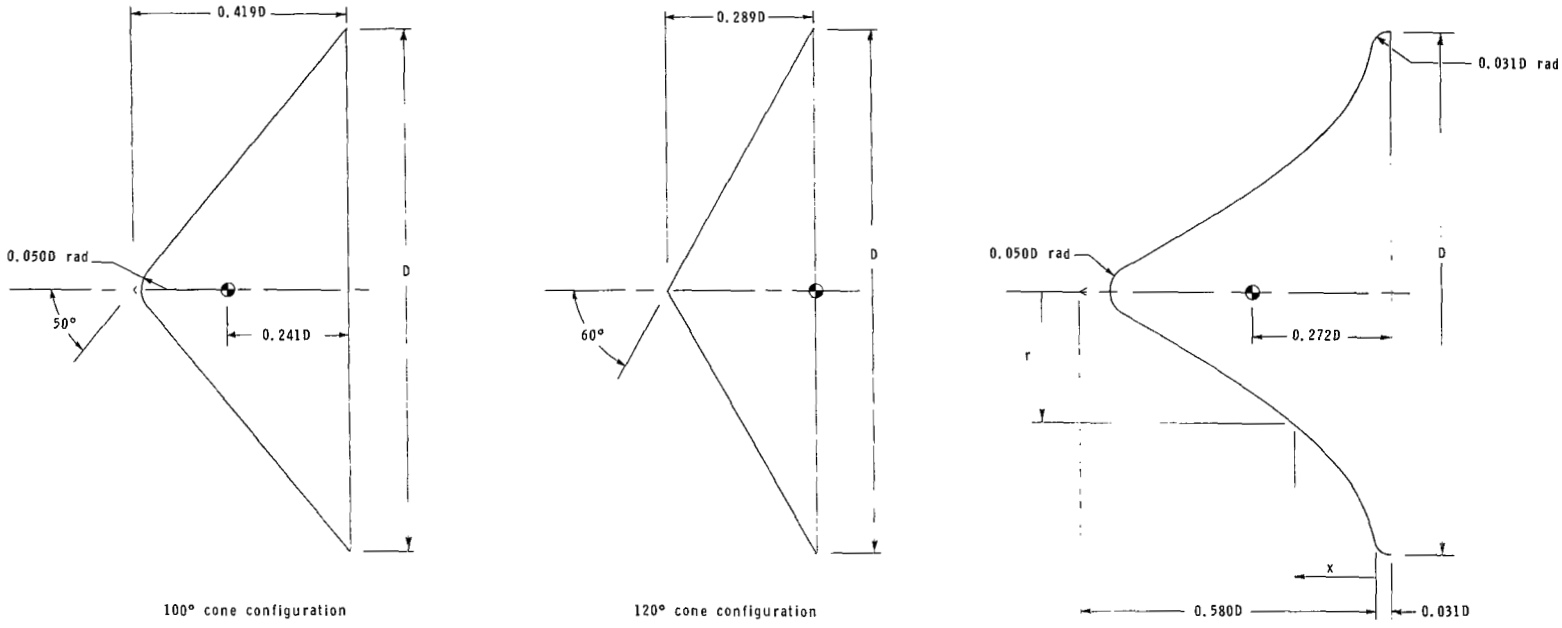

Figure 1.- Model details. (Dimensions are presented as fractions of the base diameter D; D = 8.0 in. (20.3 cm).)

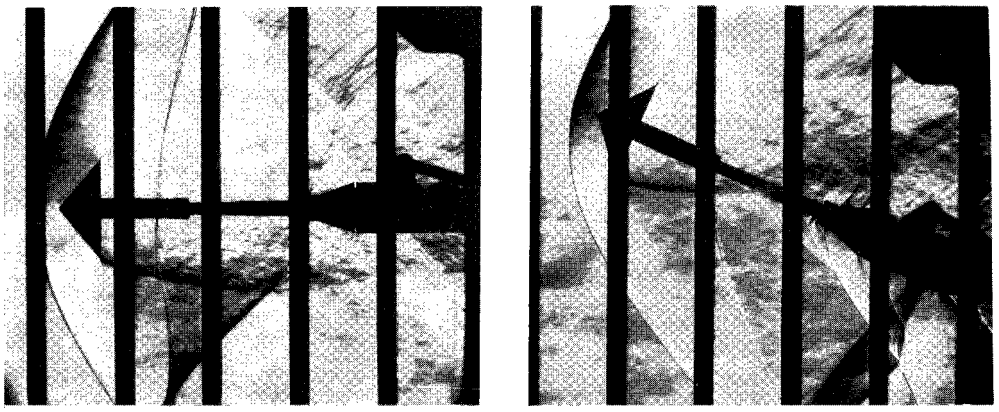

α = 0.8° α = 24.0°

(a) M = 1.50.

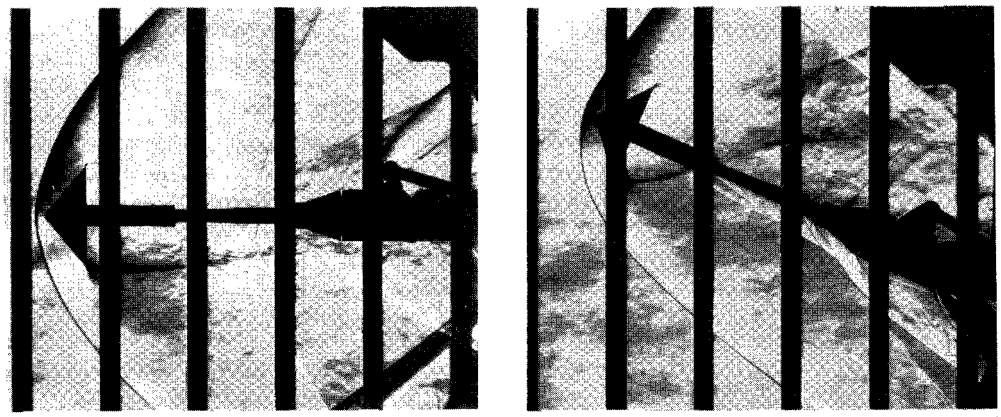

α = 1.5° α = 24.7°

(b) M = 1.90.

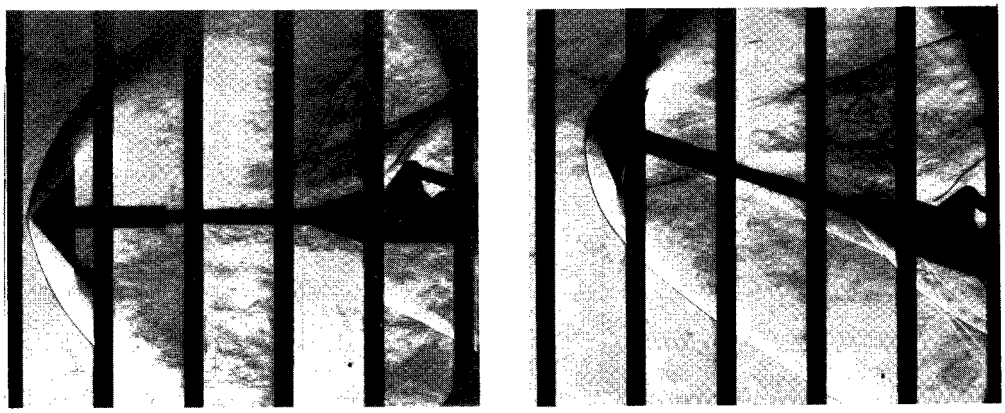

α = 0.5° α = 18.5°

(c) M = 2.30.

Figure 2.- Typical schlieren photographs of 100° cone configuration. L-67-907

$\alpha = 0.8°$

(d) M = 2.96.

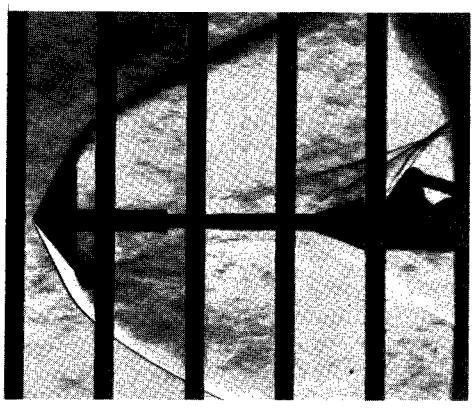

$\alpha = 0.0°$

$\alpha = 10.1°$

(e) M = 3.95.

$\alpha = 0.0°$

$\alpha = 34.2°$

(f) M = 4.63.

Figure 2.- Concluded.

L-67-908

α = 0.3°

α = 23.4°

(a) M = 1.50.

α = 1.6°

α = 24.7°

(b) M = 1.90.

Figure 3.- Typical schlieren photographs of 120° cone configuration. L-67-909

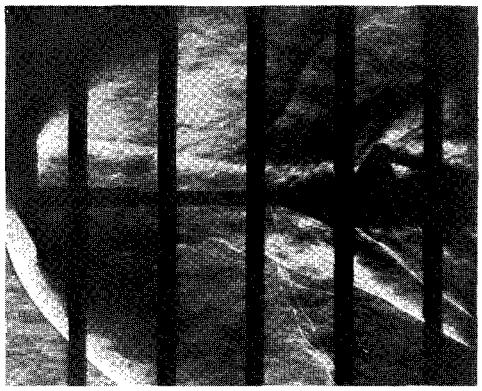

α = 1.4°

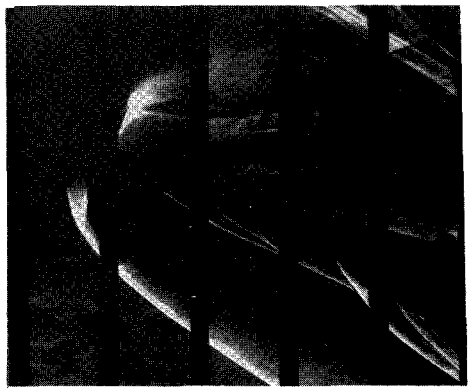

α = 23.4°

(c) M = 2.30.

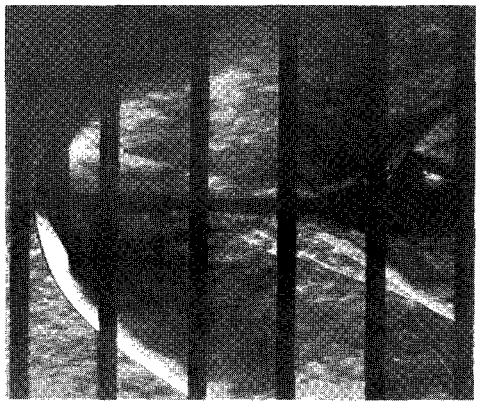

α = 1.0°

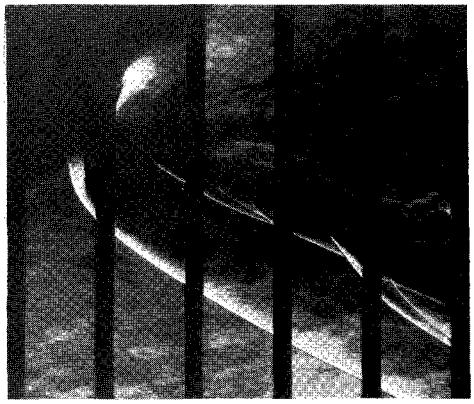

α = 23.0°

(d) M = 2.96.

α = -0.8°

α = 1.5°

(e) M = 3.95.

(f) M = 4.65.

Figure 3.- Concluded. L-67-910

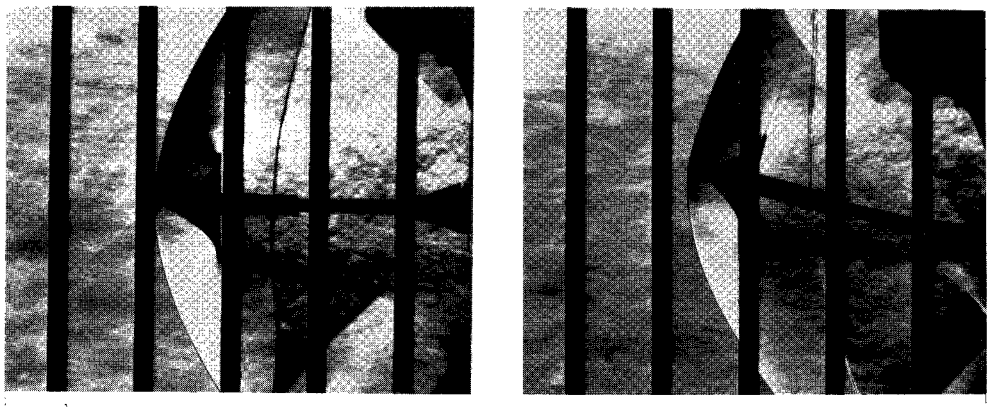

$\alpha = 0.8°$ $\alpha = 15.4°$

(a) M = 1.50.

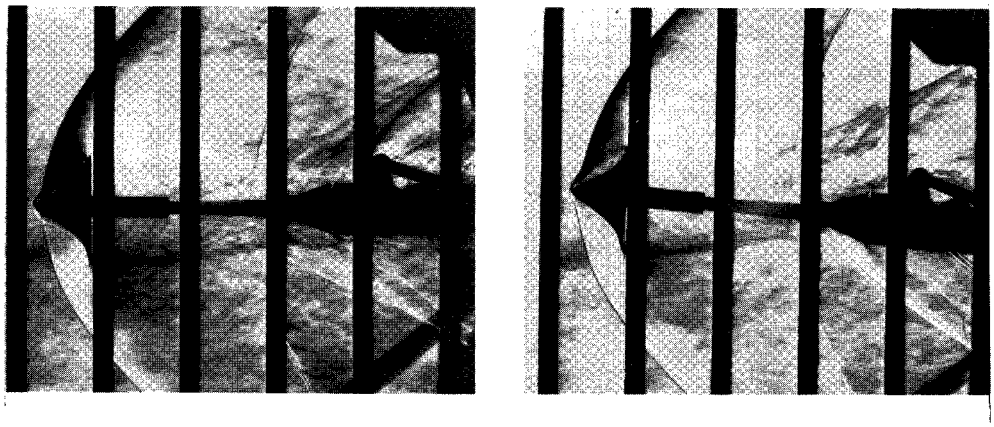

$\alpha = 0.6°$ $\alpha = 4.7°$

$\alpha = 11.1°$ $\alpha = 40.0°$

(b) M = 1.90.

Figure 4.- Typical schlieren photographs of tensoid-shape configuration. L-67-911

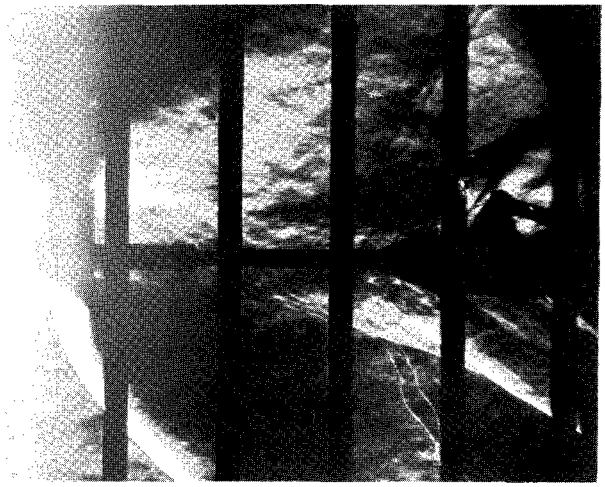

$\alpha = 0.4^\circ$

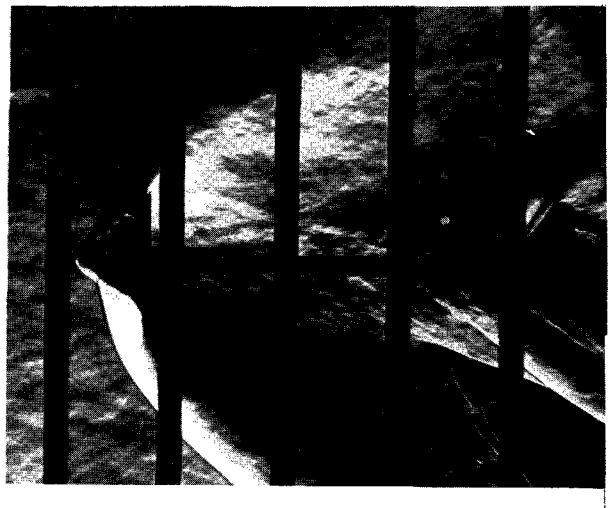

$\alpha \approx 1.3^\circ$

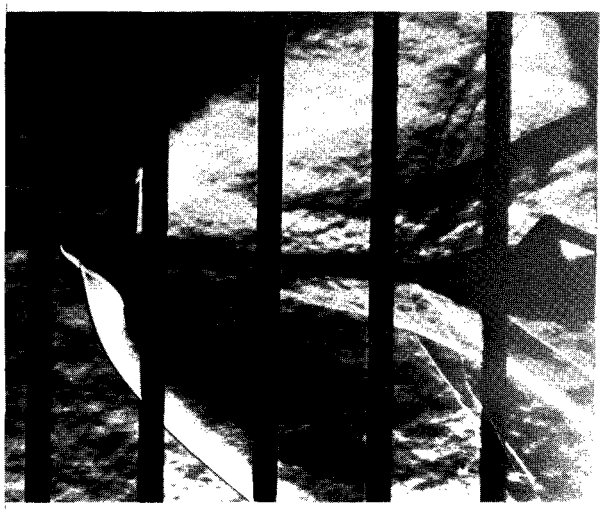

$\alpha \approx 4.5^\circ$

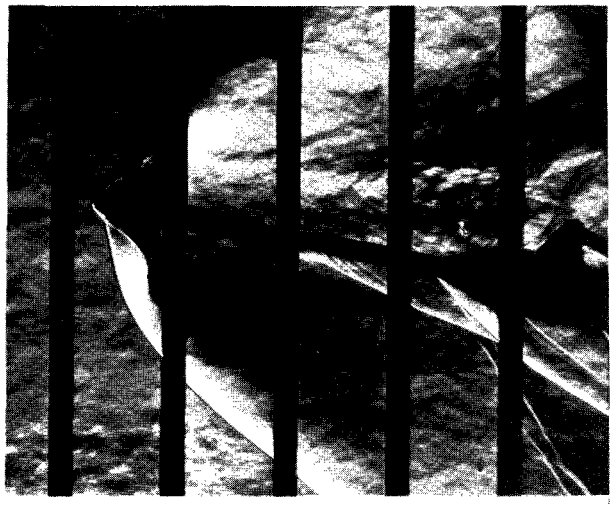

$\alpha \approx 10.5^\circ$

(c) M = 2.30.

Figure 4.- Continued. L-67-912

$\alpha = 0.1°$

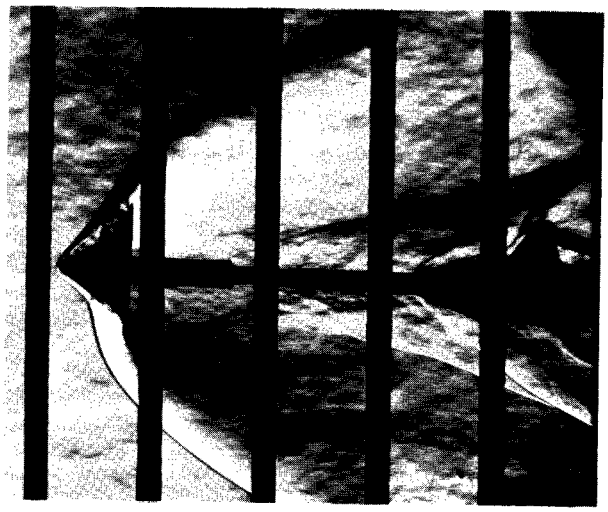

$\alpha = 2.1°$

$\alpha = 22.4°$

(d) M = 2.96.

Figure 4.- Continued.

L-67-913

$\alpha = -0.7°$

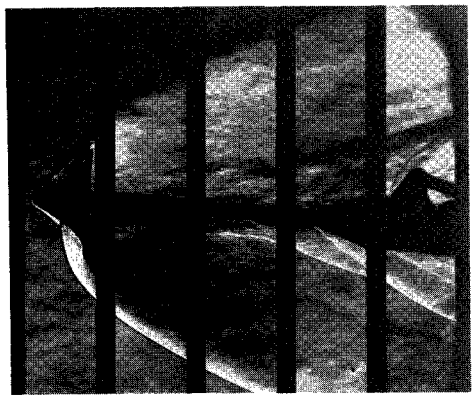

$\alpha = 4.1°$

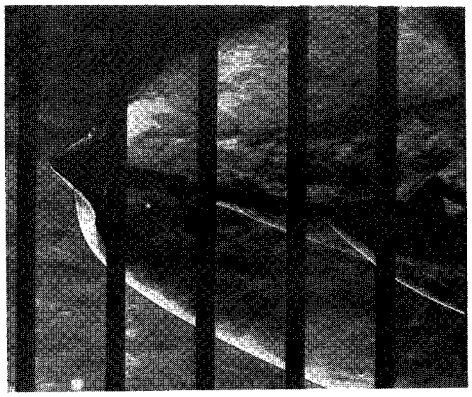

$\alpha = 10.2°$

$\alpha = 22.3°$

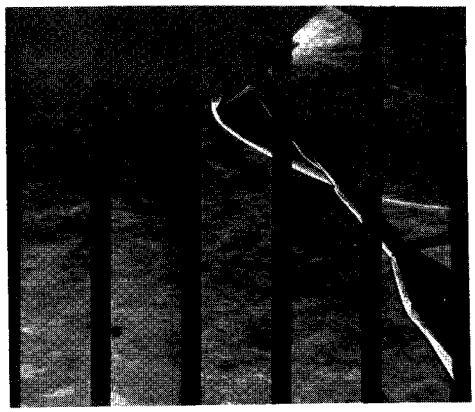

$\alpha = 50.3°$

(e) M = 3.95.

Figure 4.- Continued.

L-67-914

$\alpha = 0.5°$

$\alpha = 1.5°$

$\alpha = 2.5°$

$\alpha = 4.6°$

$\alpha = 10.7°$

(f) M = 4.63.

Figure 4.- Concluded. L-67-915

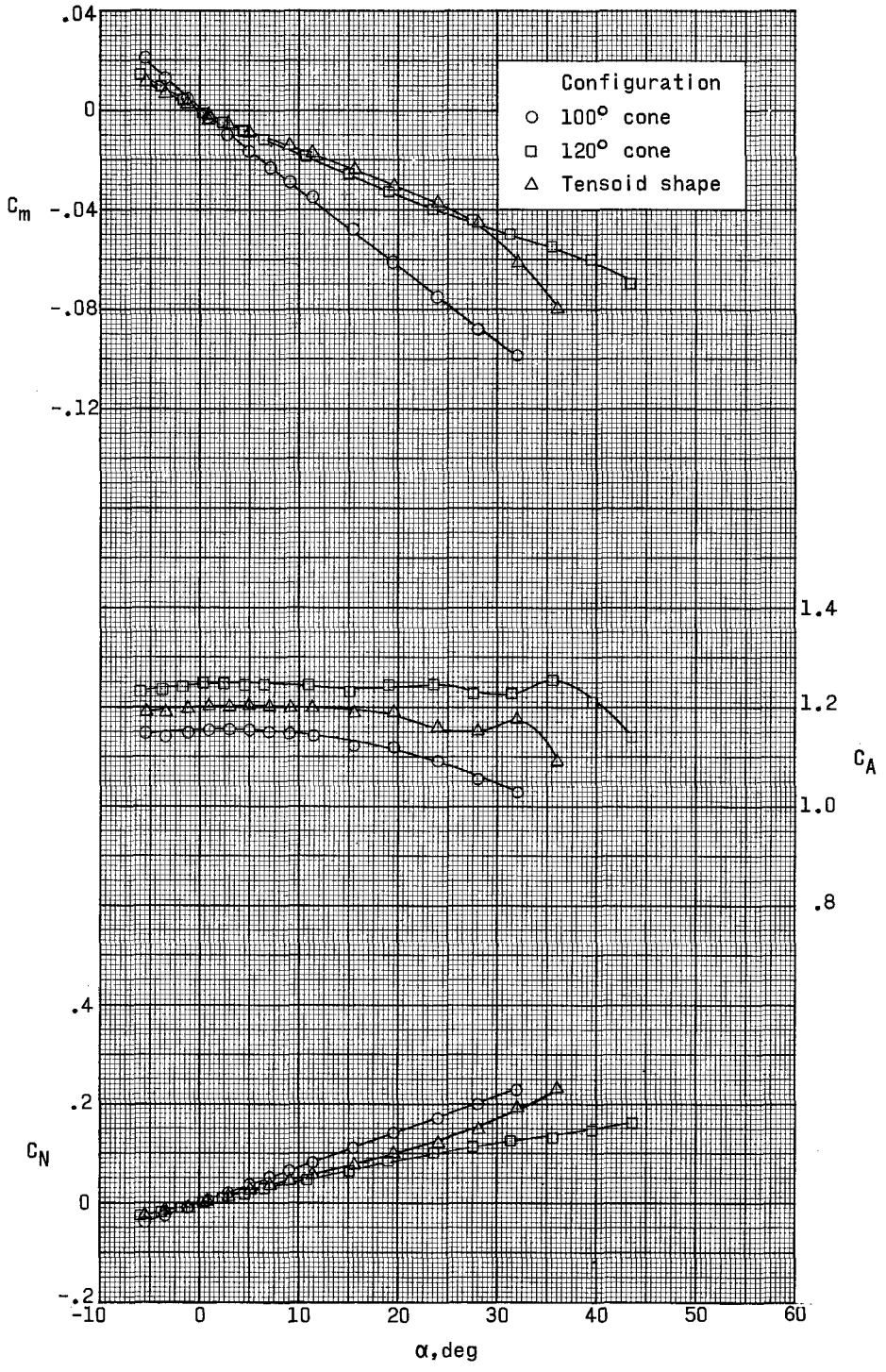

(a) M = 1.50.

Figure 5.- Variation of longitudinal characteristics (body axis) with angle of attack for test configurations.

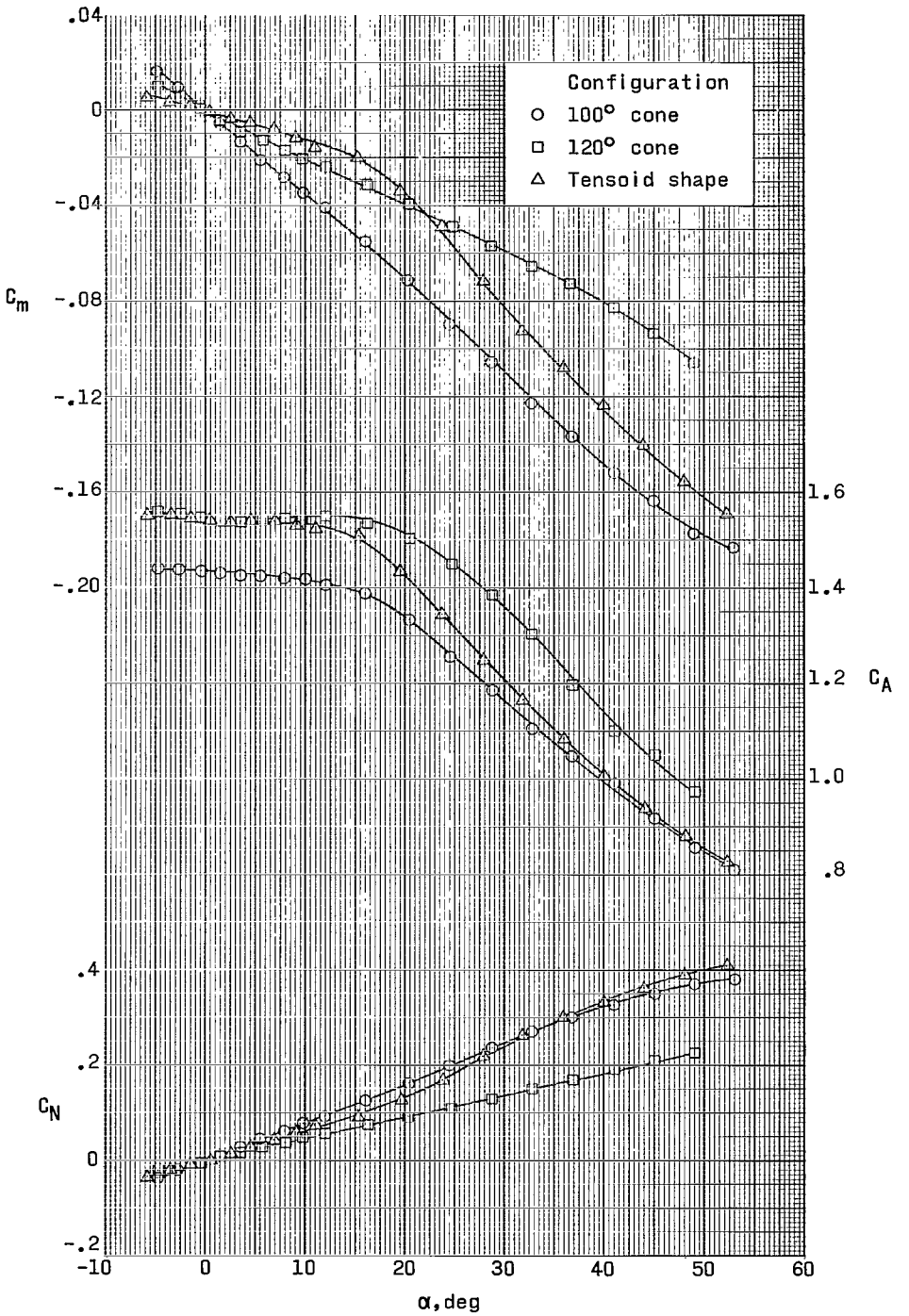

(b) M = 1.90.

Figure 5.- Continued.

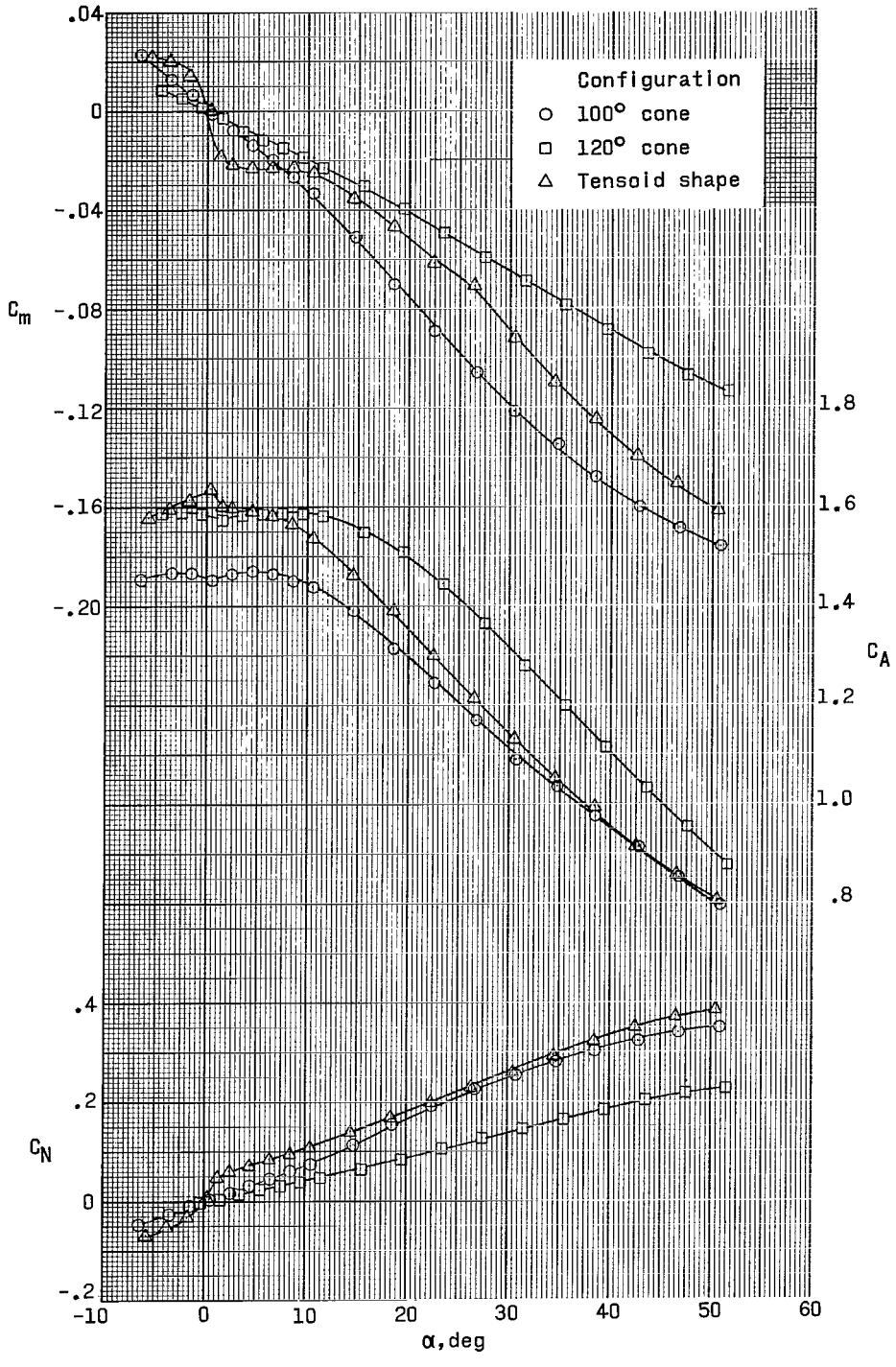

(c) M = 2.30.

Figure 5.- Continued.

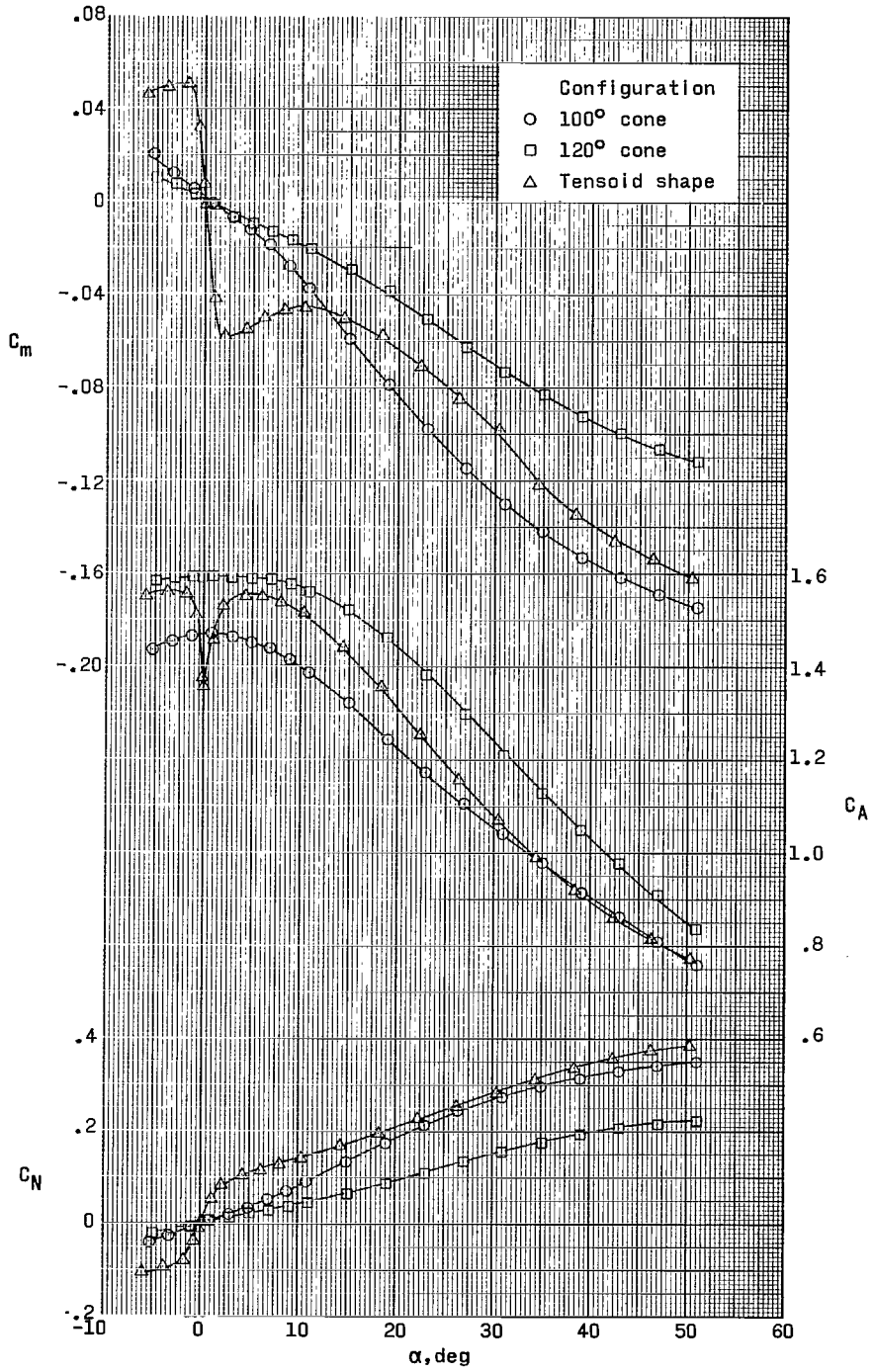

(d) M = 2.96.

Figure 5.- Continued.

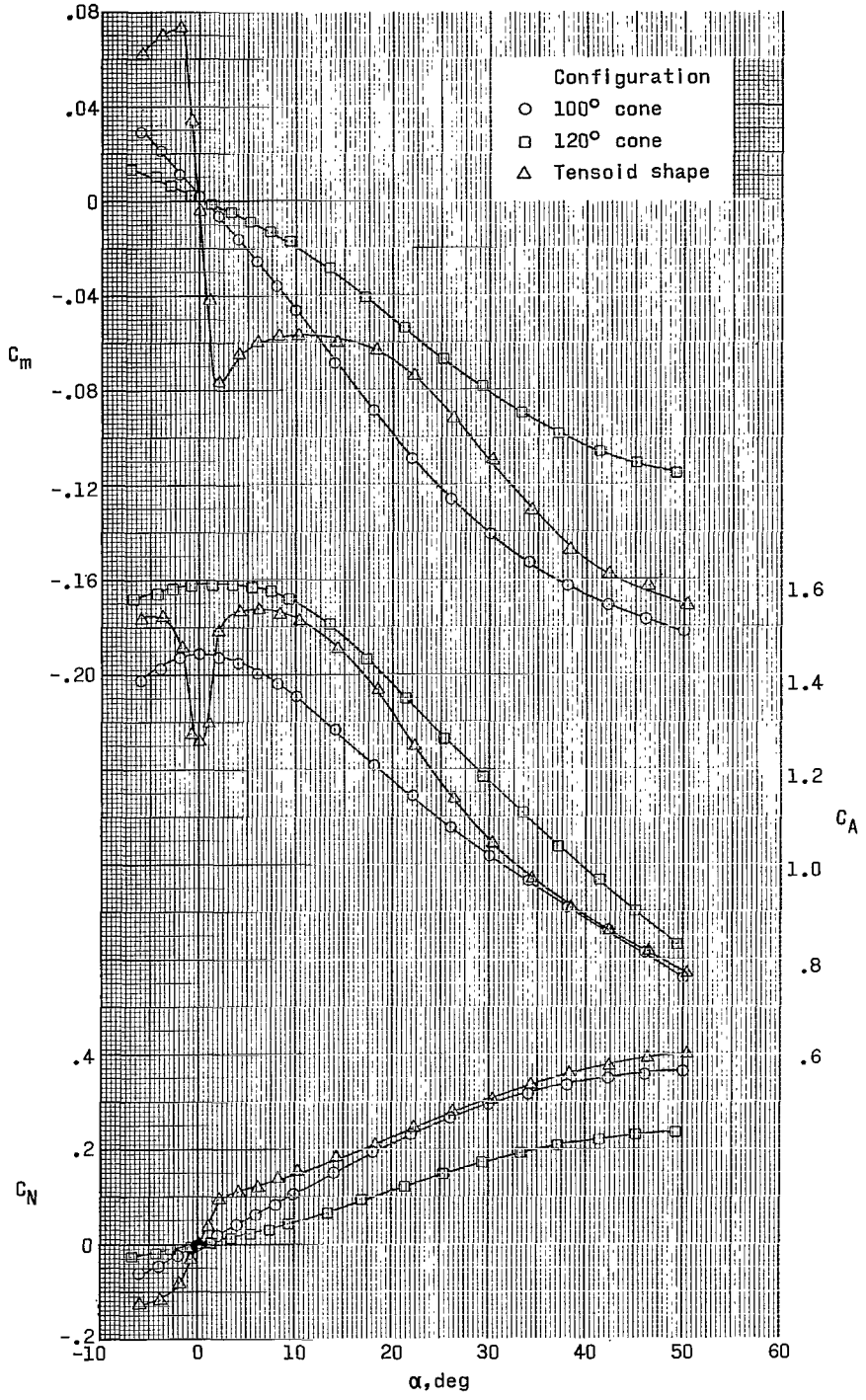

(e) M = 3.95.

Figure 5.- Continued.

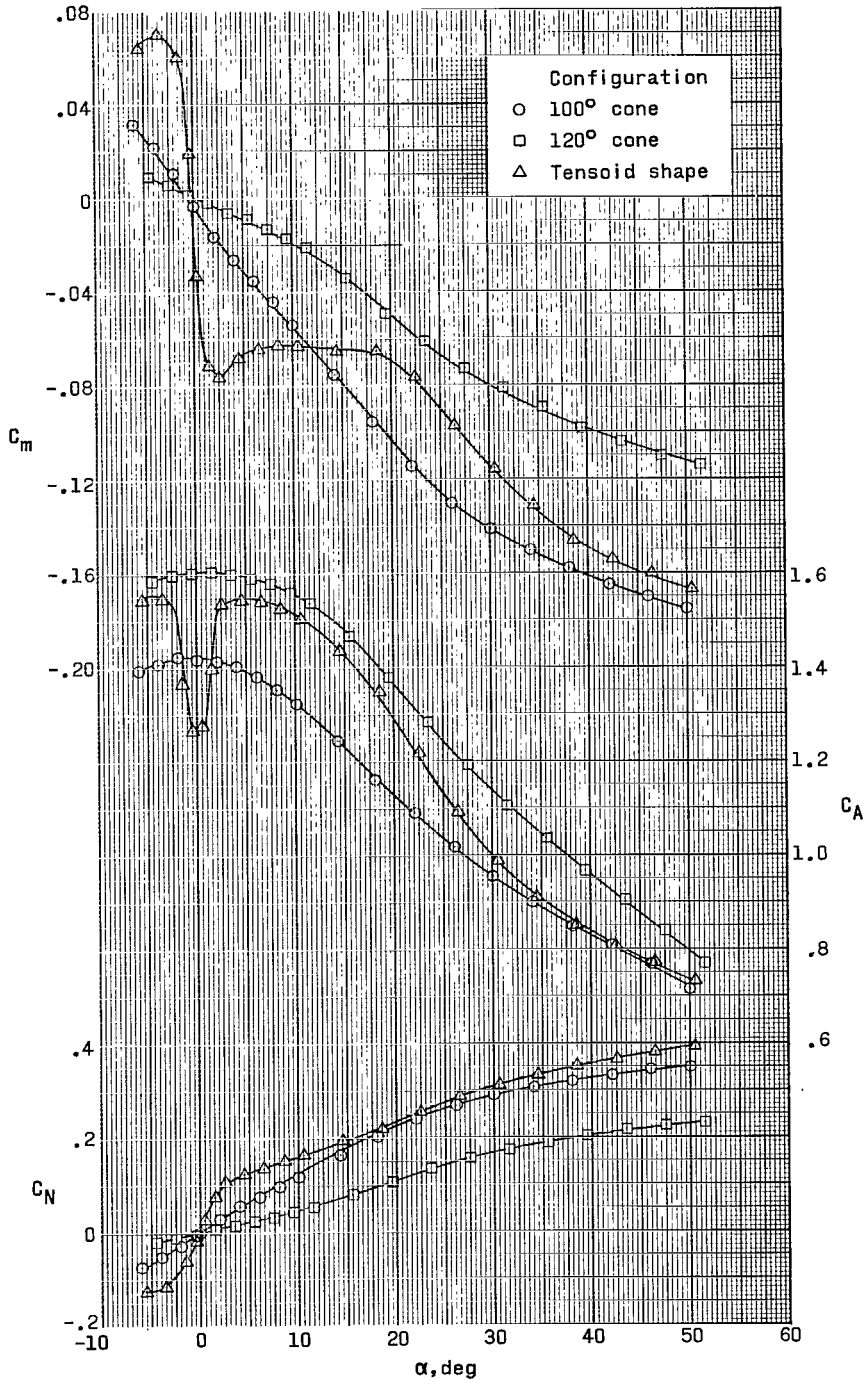

(f) M = 4.63.

Figure 5.- Concluded.

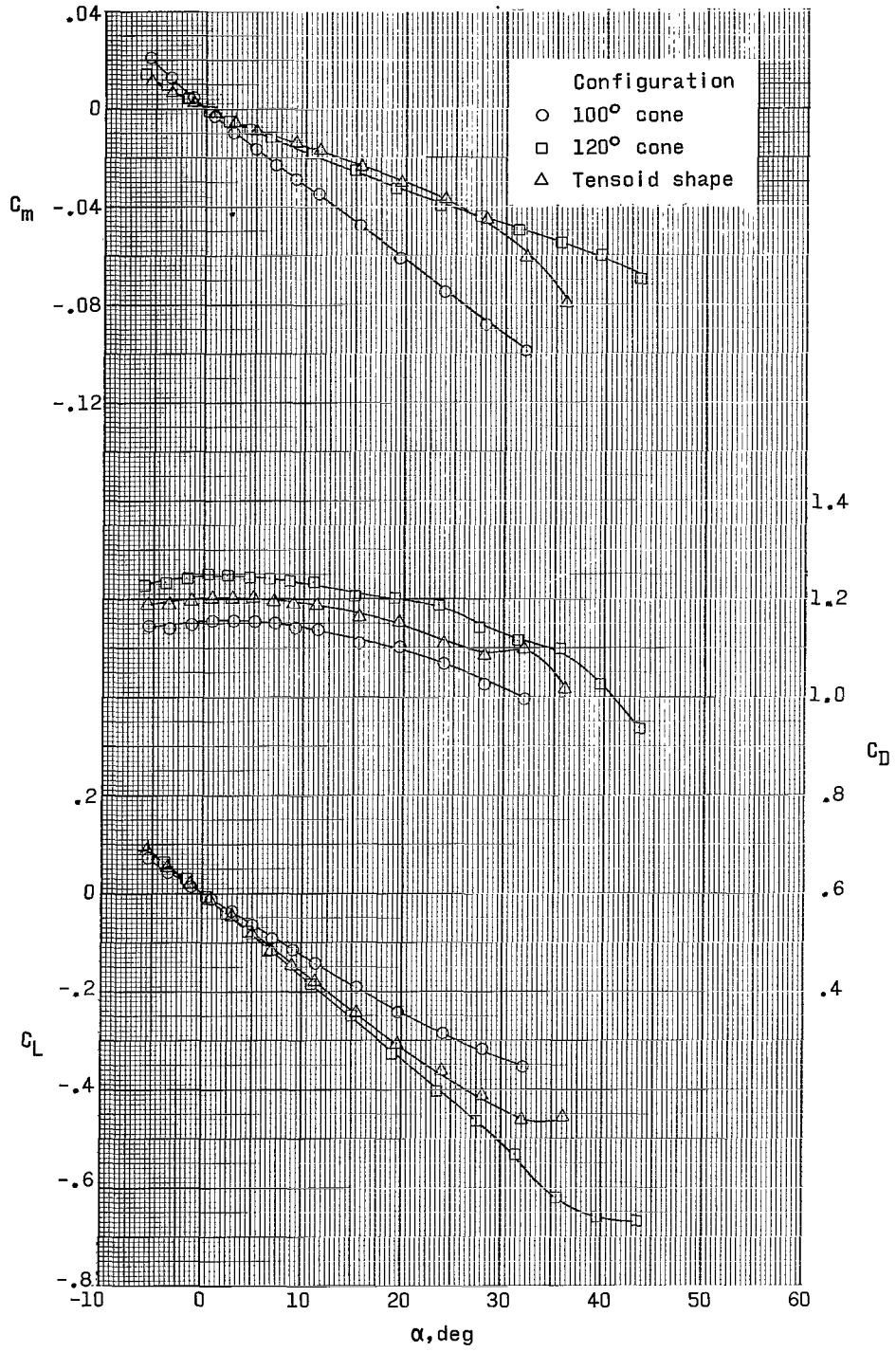

(a) M = 1.50.

Figure 6.- Variation of longitudinal characteristics (stability axis) with angle of attack for test configurations.

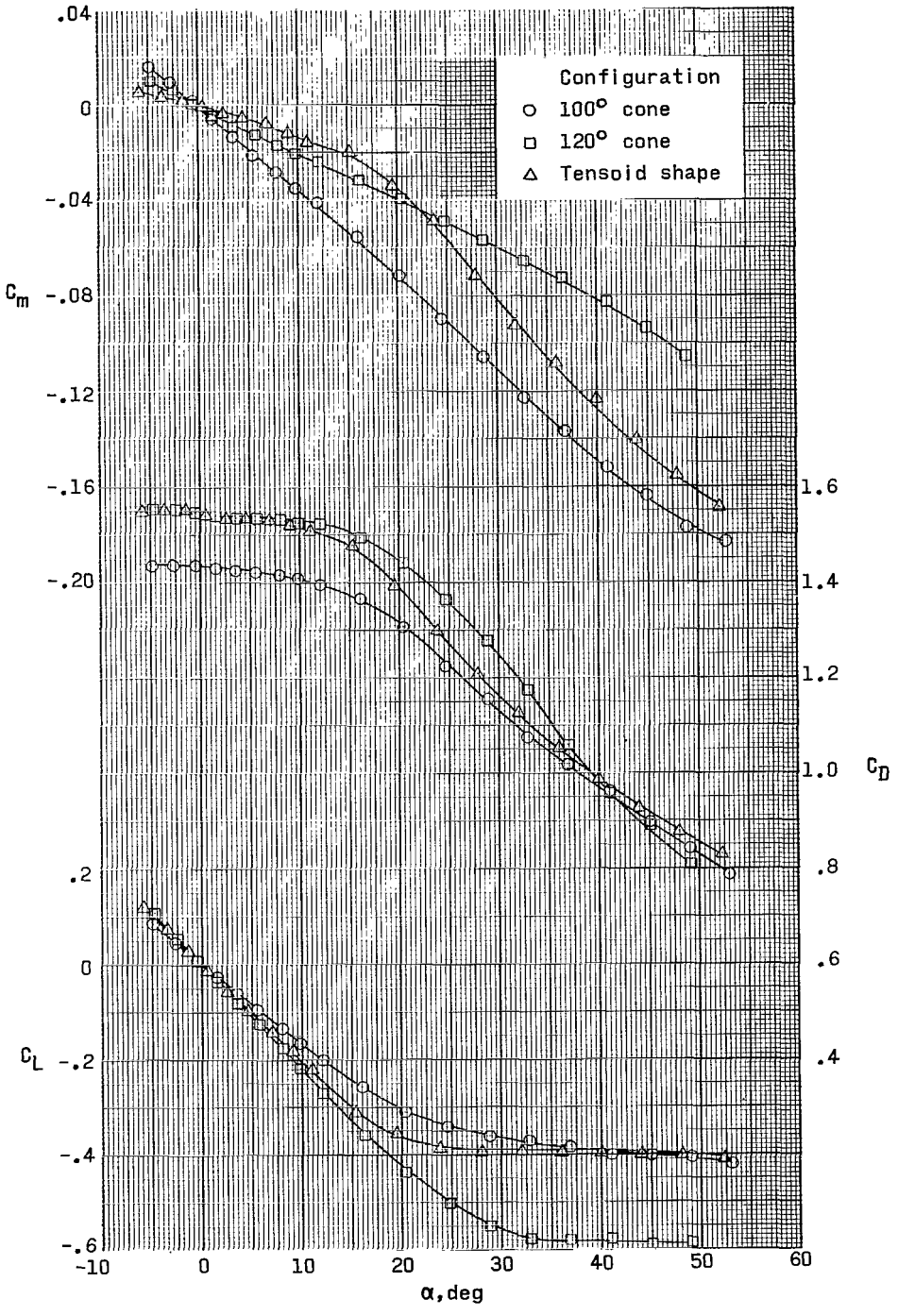

(b) M = 1.90.

Figure 6.- Continued.

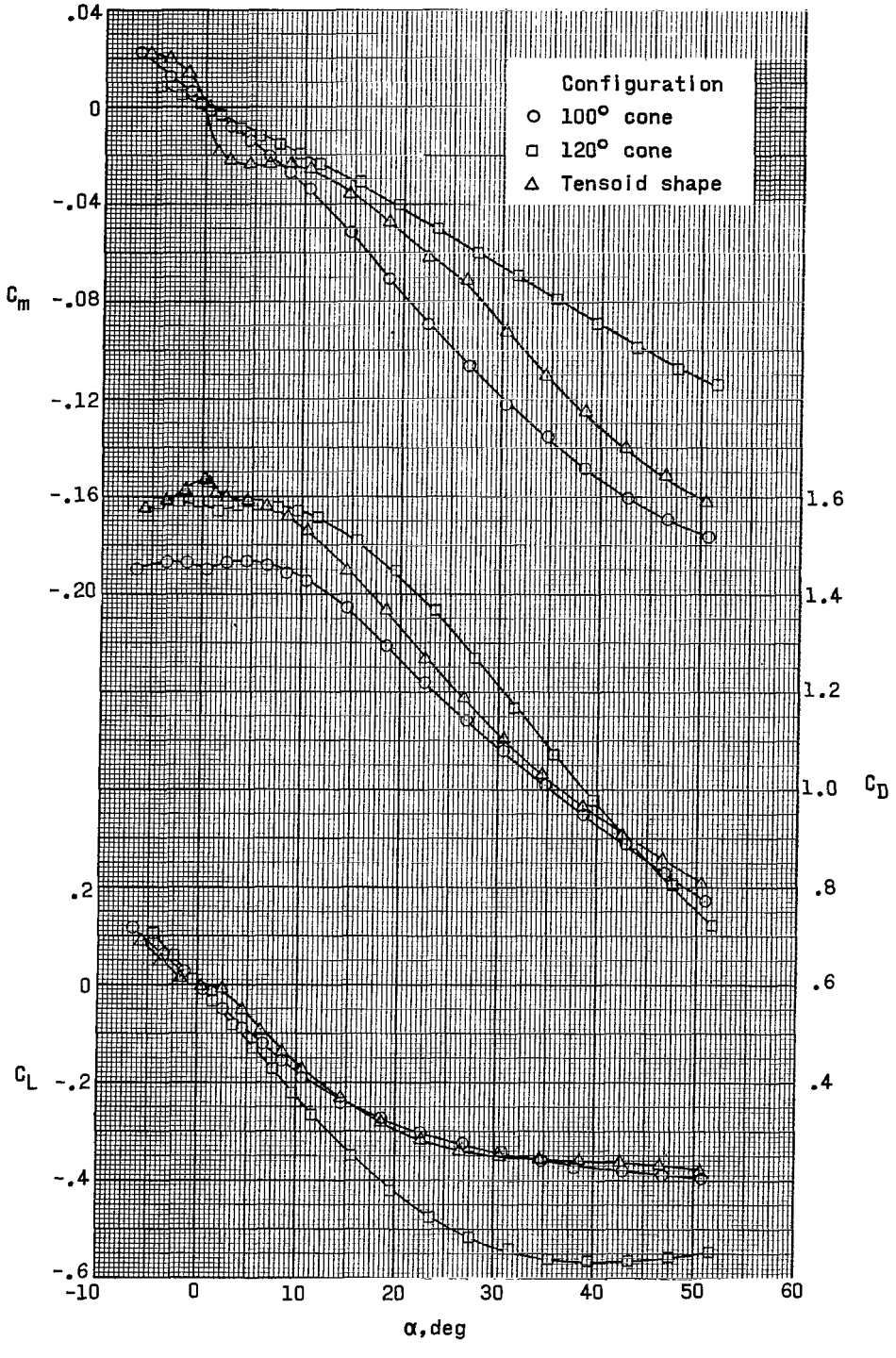

(c) M = 2.30.

Figure 6.- Continued.

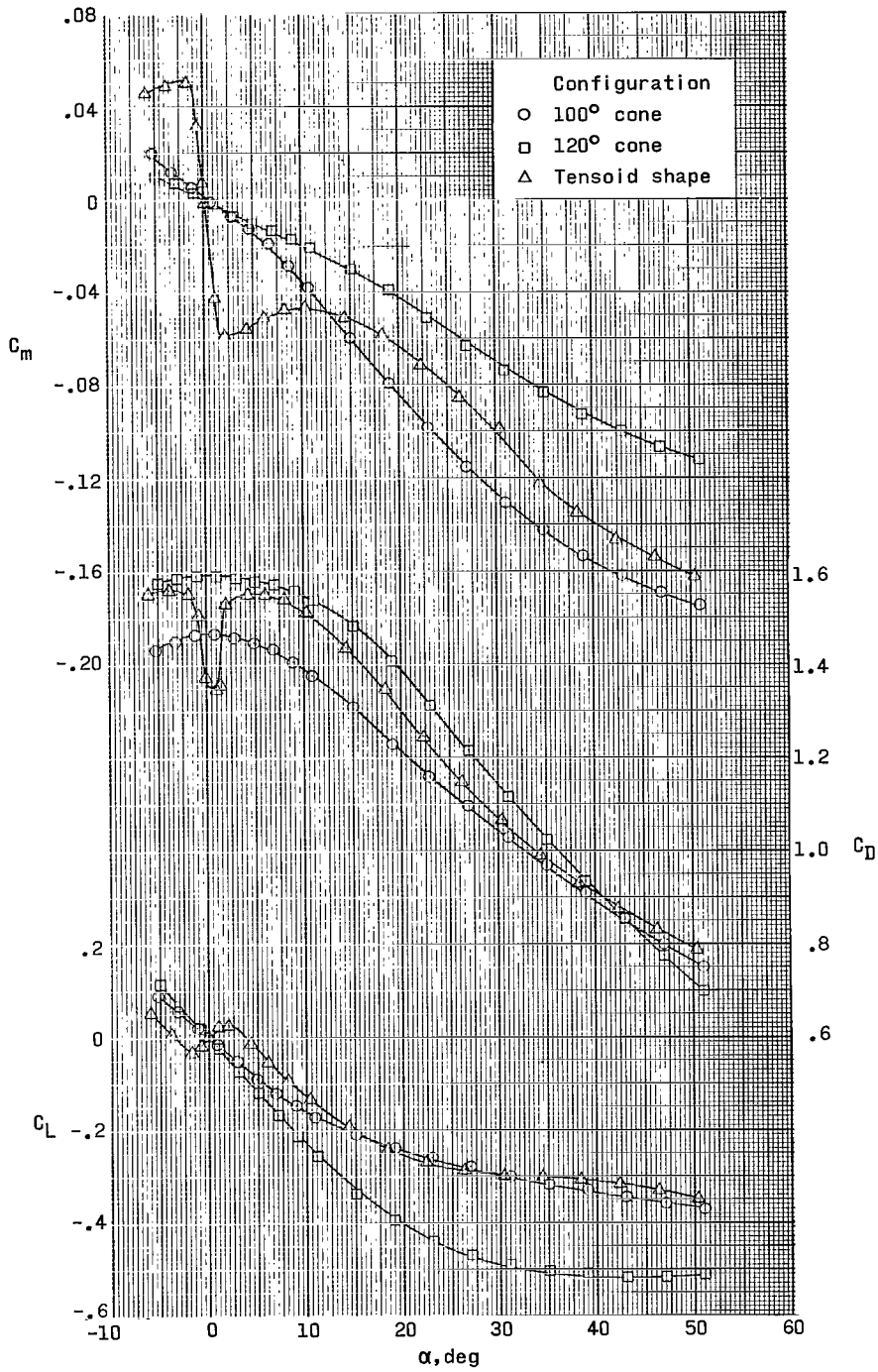

(d) M = 2.96.

Figure 6.- Continued.

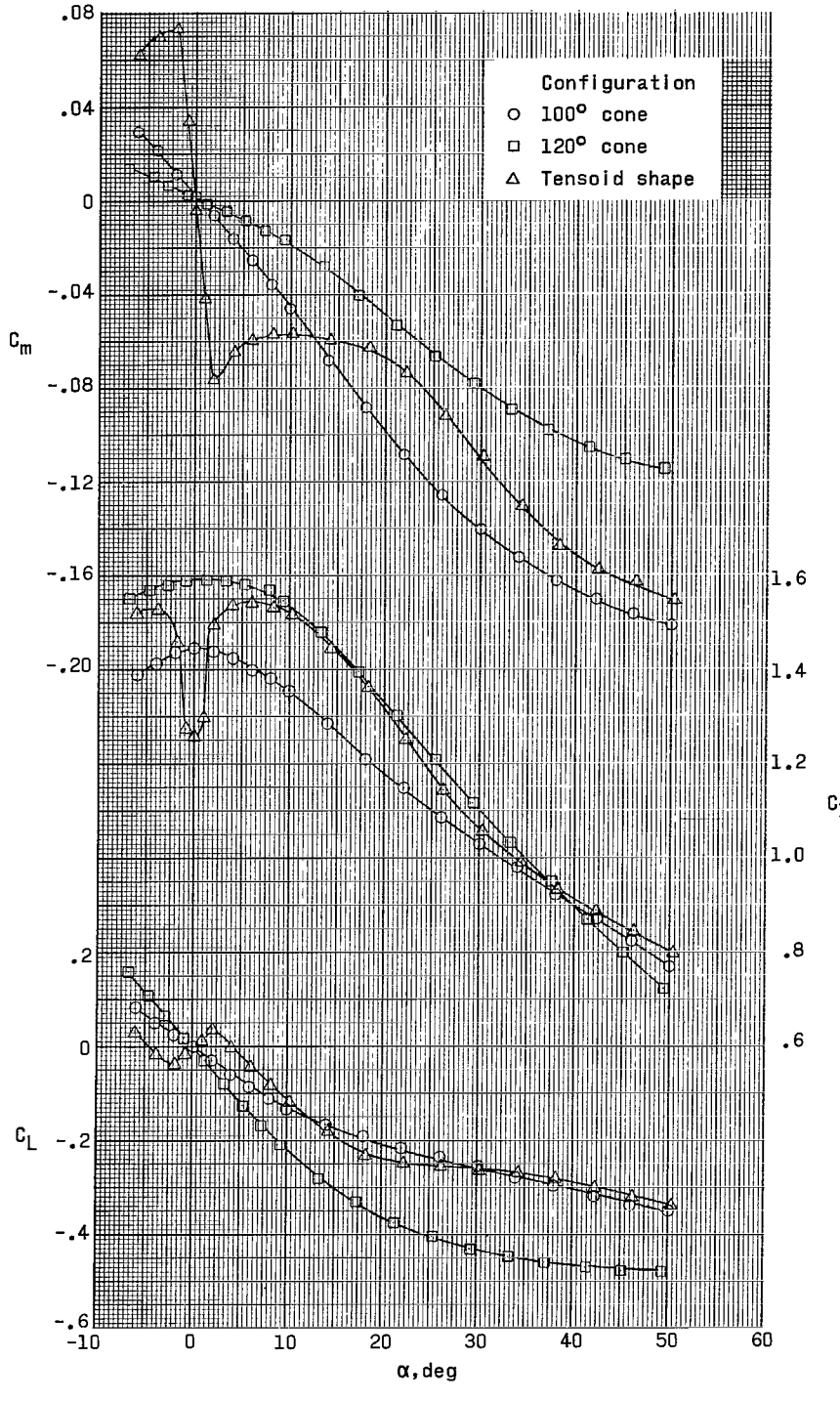

(e) M = 3.95.

Figure 6.- Continued.

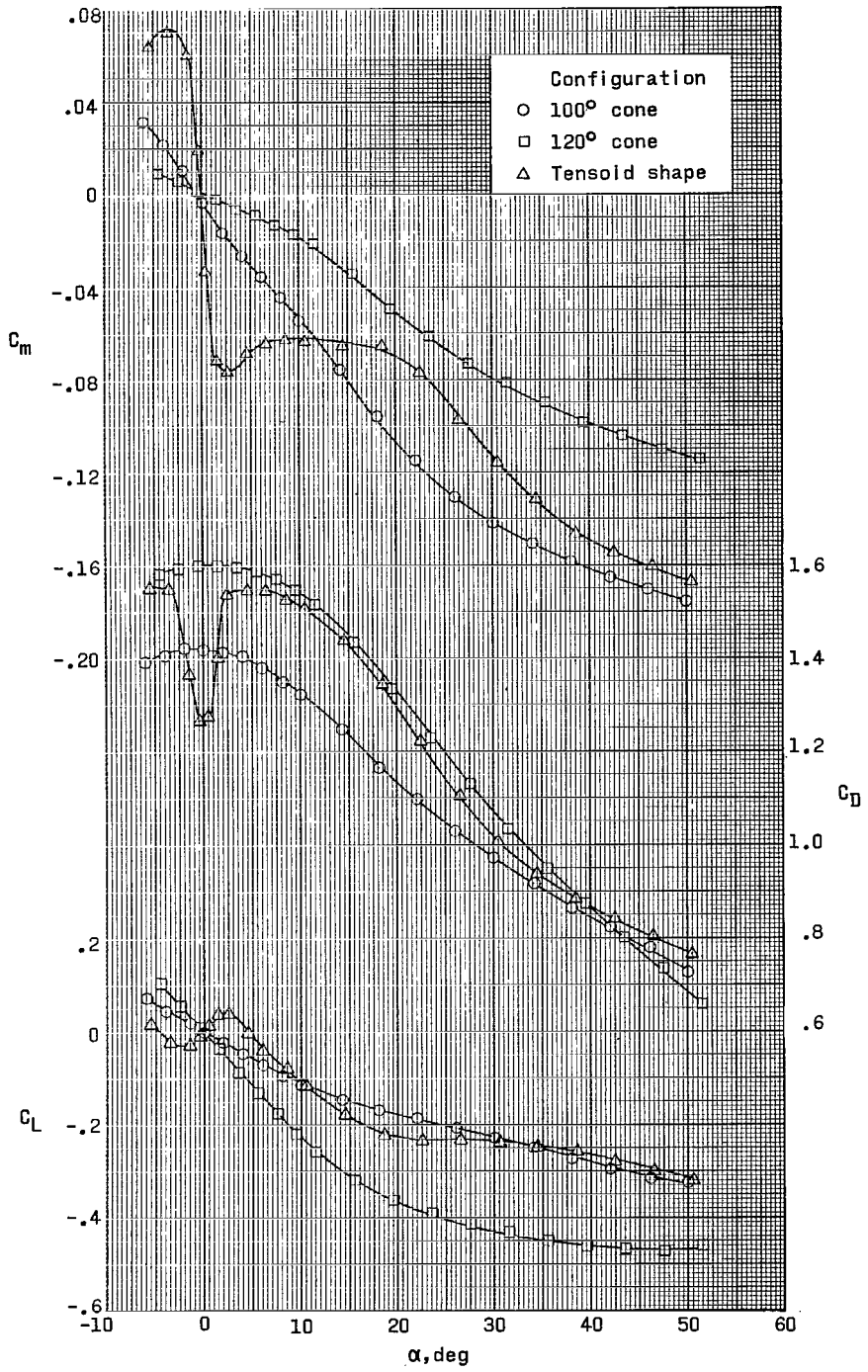

(f) M = 4.63.

Figure 6.- Concluded.

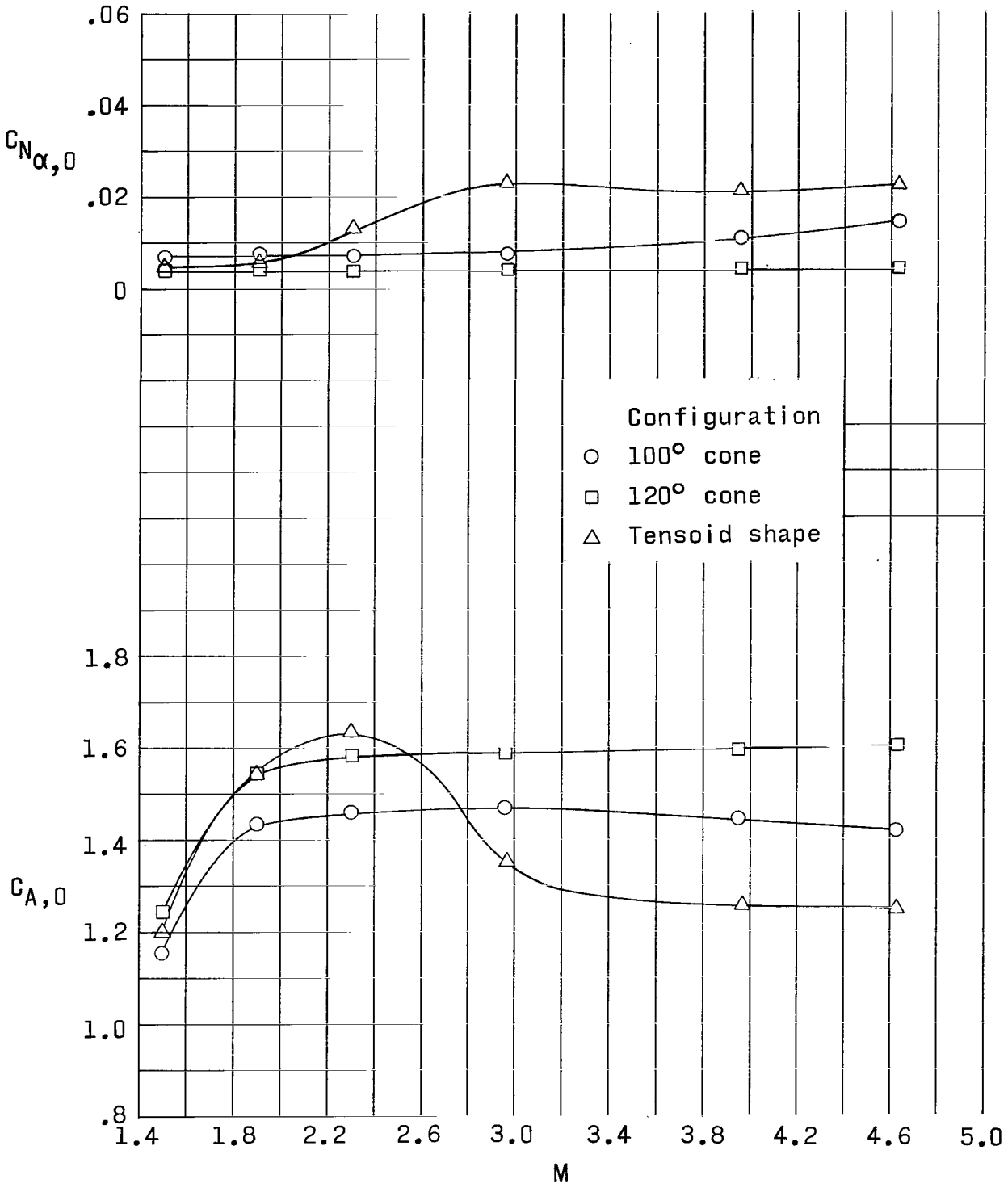

Figure 7.- Summary plot.

NASA-Langley, 1967 — 1 L-5050

"The aeronautical and space activities of the United States shall be conducted so as to contribute . . . to the expansion of human knowledge of phenomena in the atmosphere and space. The Administration shall provide for the widest practicable and appropriate dissemination of information concerning its activities and the results thereof."

—NATIONAL AERONAUTICS AND SPACE ACT OF 1958

NASA SCIENTIFIC AND TECHNICAL PUBLICATIONS

TECHNICAL REPORTS: Scientific and technical information considered important, complete, and a lasting contribution to existing knowledge.

TECHNICAL NOTES: Information less broad in scope but nevertheless of importance as a contribution to existing knowledge.

TECHNICAL MEMORANDUMS: Information receiving limited distribution because of preliminary data, security classification, or other reasons.

CONTRACTOR REPORTS: Scientific and technical information generated under a NASA contract or grant and considered an important contribution to existing knowledge.

TECHNICAL TRANSLATIONS: Information published in a foreign language considered to merit NASA distribution in English.

SPECIAL PUBLICATIONS: Information derived from or of value to NASA activities. Publications include conference proceedings, monographs, data compilations, handbooks, sourcebooks, and special bibliographies.

TECHNOLOGY UTILIZATION PUBLICATIONS: Information on technology used by NASA that may be of particular interest in commercial and other non-aerospace applications. Publications include Tech Briefs, Technology Utilization Reports and Notes, and Technology Surveys.

Details on the availability of these publications may be obtained from:

SCIENTIFIC AND TECHNICAL INFORMATION DIVISION

NATIONAL AERONAUTICS AND SPACE ADMINISTRATION

Washington, D.C. 20546